11th International Symposium on Turbulence and Shear Flow Phenomena (TSFP11)
Southampton, UK, July 30 to August 2, 2019

OUTER-LAYER DIFFERENCES IN BOUNDARY LAYER FLOW OVER SURFACES WITH REGULAR AND RANDOM ARRANGEMENTS

Kristofer M. Womack
Department of Mechanical Engineering
Johns Hopkins University
3400 N. Charles St, Baltimore, MD 21218 USA
womack@jhu.edu

Michael P. Schultz
Dept. of Naval Architecture and Ocean Engineering
United States Naval Academy
590 Holloway Rd, Annapolis, MD 21402 USA
mschultz@usna.edu

Charles Meneveau
Department of Mechanical Engineering
Johns Hopkins University
3400 N. Charles St, Baltimore, MD 21218 USA
meneveau@jhu.edu

ABSTRACT

An experimental study was conducted on rough-wall, turbulent boundary layer flow with regular and random roughness element arrangements. Varying planform densities of truncated cone roughness elements in a square staggered pattern were investigated. The same planform densities were also investigated in random arrangements. Detailed turbulent boundary layer velocity statistics were recorded with a two-component laser Doppler velocimetry system on a three-axis traverse. Important profile parameters were determined from the spatially-averaged velocity profiles for all surfaces. Evidence is presented showing that the observed differences between regular and random surface parameters are due to the presence of low momentum pathways (LMPs) and high momentum pathways (HMPs) over the random surfaces which do not seem to be present over the regular surfaces. Mechanisms which have been shown to generate and sustain LMPs and HMPs in previous studies, do not seem to be present in this study. Additionally, the LMPs and HMPs seen here are shown to be repeatable and to persist over streamwise distances. The observations of LMPs and HMPs over the random surfaces add interesting new questions about what are the salient surface morphology parameters that generate or disrupt these boundary layer scale secondary flows.

INTRODUCTION

In recent years, there has been significant study of the generation and sustainment of turbulent secondary flows. Of particular interest have been counter-rotating boundary layer scale circulation cells which cause low momentum pathways (LMPs) and high momentum pathways (HMPs) in the mean streamwise velocity due the their vertical transport of momentum and other turbulence quantities throughout the boundary layer. LMPs and HMPs occur in the mean flow and are distinct from low momentum regions and high momentum regions which occur in the instantaneous velocity field (Barros & Christensen (2014)).

Barros & Christensen (2014) first reported spanwise alternating LMPs and HMPs in the mean streamwise velocity over a complex surface which were also marked by elevated and depressed quantities of Reynolds shear stresses and turbulent kinetic energy (TKE), respectively. They reported that these LMPs and HMPs seemed to correlate with low and high average surface roughness elevation in the one boundary layer thickness, δ, streamwise fetch immediately upstream of the measurement location. Anderson *et al.* (2015) reported similar findings in flow over a striped roughness with alternating spanwise regions of higher and lower peak-to-trough roughness height, k. They studied the TKE and vorticity transport equations and determined that higher TKE production over the higher k areas caused and sustained the secondary flows.

There is an assumption that real world flows over complex and random surfaces do not generate and sustain secondary flows. Therefore, computations and experiments which have general application should not have secondary flows. That makes criteria predicting LMPs and HMPs of practical interest when designing experiments with the widest relevance. In an effort to quantify such criteria, recent work by Vanderwel & Ganapathisubramani (2015) found δ-scale circulations were not significant on their surfaces when spanwise spacing is less than $\delta/2$.

These recent studies have focused attention on LMP and HMP dependencies on the spanwise spacing of roughness features, especially for cases when the surface has a repeated pattern generating the streamwise structures. In contrast, for random surfaces and in facilities and flows of sufficient size, the absence of repeated surface patterns leads to the expectation that such structures are less likely to form. In this paper, we report a series of experiments where the regular surfaces do not appear to exhibit LMPs and HMPs. However, the random surfaces appear to generate and sustain LMPs and HMPs over at least 4δ of streamwise fetch. We report regular and random surface spatially-averaged boundary layer results, highlight differences between the regular and random surface results, and add new data to the body of information regarding LMPs and HMPs.

EXPERIMENTAL METHODS

Experiments were conducted at the Hydromechanics Laboratory at the United States Naval Academy in a recirculating water tunnel. The test section is nominally 2.00 m long with a 0.20 m wide by 0.10 m tall cross-section at the inlet. The upper wall was adjusted to set a zero pressure gradient, and the resulting acceleration parameter, $K = (\nu/U_e^2)[dU_e/dx]$, was less than 5×10^{-9} throughout the length of the test section for each test. All tests were conducted with the free-stream velocity of $U_e = 1.25$ m/s. In this study, (x, y, z) were the streamwise, wall-normal, and spanwise directions respectively, and u, v, w were the streamwise, wall-normal, and spanwise velocities respectively. $y = 0$ was located on the lower surface to which the roughness elements were attached, and $z = 0$ was located at the center of the cross-section. A 0.8 mm diameter wire trip was located 0.20 m from the tunnel inlet and served as the streamwise origin, $x = 0$. The roughness field began 0.78 m from the boundary layer trip, and velocity measurements were recorded nominally 1.50 m from the trip which was approximately 19δ from the start of the roughness. A heat pump system controlled fluid temperature to $20 \pm 1\,^{\circ}$C during tests, which in some cases lasted over 50 hours.

Sixteen test surfaces were constructed using high resolution additive manufacturing with a Stratasys Objet30 Pro 3D printer. Eight cases had varying planform densities of truncated cone elements in a square staggered pattern. In the most dense case the truncated cone elements were touching but not overlapping at the base. The same eight planform densities were manufactured with random arrangements of the truncated cone elements. In the random cases the elements may overlap but a minimum of 0.5 mm was maintained between the elements' upper plateaus. The base diameter of the truncated cone was $D = 6.96$ mm, and the top diameter was $0.400D = 2.78$ mm. The truncated cone height was $k = 0.453D = 3.15$ mm. Cases were named with an 'S' for staggered or 'R' for random and then two digit percentage for the planform density. Selected surface statistics for all surfaces are documented in Table 1.

Detailed turbulent boundary layer statistics were recorded with a TSI two-component Laser Doppler Velocimetry (LDV) system. For the square staggered cases, nine wall-normal profiles were recorded at representative locations over a repeating unit. Each profile contained 50 sampling locations in the y-direction where velocity data was recorded for 180 seconds. For the random cases, 12 wall-normal profiles were recorded and spaced at $1.5D$ across the span of the tunnel. This spacing and number of profiles allowed statistically independent profiles and well-converged spanwise averages to be evaluated for most profiles. Additional tests were performed for the R17 and R39 cases with 23 profiles spaced at $0.75D$ since these profiles appeared less well-converged. Each of the 12 or 23 profiles contained 50 sampling locations in the y-direction where velocity data were recorded for 150 seconds.

RESULTS

Spatially-averaged boundary layer results

The log-law equation for rough walls can be written as

$$U^+ = \frac{1}{\kappa}\ln\left(\frac{y-d}{y_0}\right) + \frac{\Pi}{\kappa}W\left(\frac{y}{\delta}\right) \qquad (1)$$

where U^+ is the mean streamwise velocity normalized by friction velocity (u_τ), κ is the Kármán constant, y_0 is the roughness length, d is the zero-plane displacement, Π is the wake strength parameter, and $W\left(\frac{y}{\delta}\right)$ is the wake function.

Experimental boundary layer profiles were analyzed with the comprehensive shear stress method described in Womack *et al.* (2019). In each iteration, a spatially-averaged version of the Volino & Schultz (2018) equation (a version of the total shear stress balance) was fitted in the range of $0.15 < (y-d)/(\delta-d) < 0.30$ to determine u_τ, and Eq. 1 was fitted in the range of $0.07 < y/\delta < 0.15$ to determine y_0 and d. The Kármán constant was assumed to be $\kappa = 0.384$. The convergence criteria for each profile were three significant digits in u_τ and y_0 or 10 iterations. Table 2 contains results from the comprehensive shear stress method as well as other relevant profile parameters for each surface's spatially-averaged profile. k_s is related to y_0 by the equation $k_s = y_0 e^{8.5\kappa}$. The momentum thickness, θ, was calculated using trapezoidal integration and adding a point with $U^+ = 0$ at the wall.

Inner-normalized spatially-averaged mean streamwise velocity profiles are plotted in Fig. 1. The dashed black line shows the smooth-wall log-law with $\kappa = 0.384$ and $B = 4.17$. All profiles show the expected downward shift due to roughness effects. The S10, R10, S17, and R17 cases have clearly less downward shift than the other cases, which plot together more closely. All sixteen average profiles exhibit a log-linear region with slope of about $1/\kappa$ between approximately $0.07 < y/\delta < 0.15$. The existence of a logarithmic region in data with similar or larger ratios of roughness height to boundary layer thickness has been seen in other studies such as Placidi & Ganapathisubramani (2015) among others.

Comparison of regular and random surfaces

Individual mean streamwise velocity profiles for the S78 staggered case are plotted in Fig. 2a, and individual mean streamwise velocity profiles for R78 random case are plotted in Fig. 2b. The spatial average is plotted with a thick black line in each figure. It is clear from Fig. 2a that the various S78 individual profiles converge within one roughness height, k, above the roughness crests. This is the result for all staggered cases in this study and is consistent with other studies where differences are confined below $5k$ (Flack *et al.* (2005); Placidi & Ganapathisubramani (2015)). In contrast, Fig. 2b shows visual differences in the individual profiles to the edge of the boundary layer. This is similar to the result for all random cases in this study.

Mean velocity profiles in defect form are included for all staggered cases in Fig. 3a and for all random cases in Fig. 3b. DNS at $\mathrm{Re}_\tau \approx 2000$ from Sillero *et al.* (2013) is included as the thick black dotted line for reference in both plots. All staggered cases except S10 plot above the DNS reference in Fig. 3a, and all random cases plot near the DNS reference in Fig. 3b. Additionally, there is a greater visual spread in the profiles at low $(y-d)/(\delta-d)$ for the staggered cases when compared to the random cases. Further evidence of the differences seen in Fig. 3 is found in the column of Π values in Table 2. For the staggered cases, wake strength ranges from $\Pi = 0.53 - 0.79$ compared with $\Pi = 0.51 - 0.66$ for the random cases. The differences in wake strength are largely outside of the experimental uncertainty.

The increase above traditionally accepted values of wake strength and the greater spread in the staggered cases'

Table 1: Test surface statistics

Case	λ_p	λ_f	Effective slope	Mean, $\langle h \rangle$ (mm)	St. deviation, σ_h (mm)	Skewness	Flatness
S10	0.098	0.040	0.079	0.16	0.59	3.956	18.0
S17	0.175	0.070	0.141	0.29	0.76	2.756	9.46
S39	0.393	0.159	0.317	0.64	1.03	1.409	3.52
S48	0.485	0.196	0.391	0.79	1.09	1.095	2.70
S57	0.565	0.228	0.457	0.93	1.13	0.869	2.26
S63	0.631	0.255	0.509	1.03	1.15	0.709	2.01
S70	0.698	0.282	0.564	1.14	1.15	0.561	1.84
S78	0.785	0.317	0.634	1.29	1.14	0.393	1.71
R10	0.098	0.040	0.079	0.16	0.59	3.921	17.7
R17	0.174	0.070	0.140	0.29	0.77	2.709	9.15
R39	0.392	0.155	0.310	0.68	1.07	1.311	3.20
R48	0.484	0.190	0.379	0.86	1.14	0.960	2.36
R57	0.565	0.220	0.440	1.03	1.18	0.690	1.91
R63	0.630	0.243	0.486	1.16	1.20	0.498	1.69
R70	0.697	0.266	0.532	1.31	1.21	0.294	1.54
R78	0.785	0.296	0.591	1.53	1.19	0.035	1.51

Table 2: Spatially-averaged profile parameters

Case	Re_τ	U_e (m/s)	u_τ (m/s)	θ (mm)	$\frac{d}{k}$	$\frac{y_0}{k}$	$\frac{k}{\delta-d}$	$\frac{k_s}{\delta-d}$	k_s^+	Π
S10	2090	1.253	0.068	4.5	0.40	0.027	0.102	0.072	151	0.53
S17	2410	1.251	0.072	5.1	0.36	0.048	0.094	0.118	286	0.60
S39	2780	1.255	0.075	5.8	0.29	0.094	0.084	0.208	578	0.75
S48	2750	1.254	0.076	5.8	0.44	0.091	0.086	0.205	563	0.73
S57	2680	1.251	0.076	5.6	0.58	0.081	0.088	0.186	500	0.68
S63	2640	1.256	0.074	5.7	0.59	0.080	0.088	0.183	484	0.74
S70	2490	1.253	0.073	5.6	0.66	0.070	0.090	0.165	410	0.73
S78	2490	1.249	0.073	5.6	0.62	0.081	0.091	0.193	481	0.79
R10	2110	1.258	0.069	4.5	0.40	0.026	0.102	0.069	145	0.51
R17	2420	1.255	0.074	4.9	0.16	0.054	0.095	0.135	327	0.61
R39	3050	1.253	0.082	5.7	0.23	0.098	0.083	0.214	654	0.52
R48	2830	1.252	0.078	5.6	0.44	0.091	0.087	0.206	582	0.62
R57	2800	1.252	0.078	5.6	0.59	0.082	0.087	0.187	524	0.59
R63	2840	1.254	0.079	5.7	0.53	0.083	0.087	0.190	538	0.56
R70	2730	1.253	0.078	5.5	0.46	0.094	0.090	0.221	602	0.66
R78	2680	1.258	0.075	5.6	0.58	0.068	0.088	0.156	419	0.62

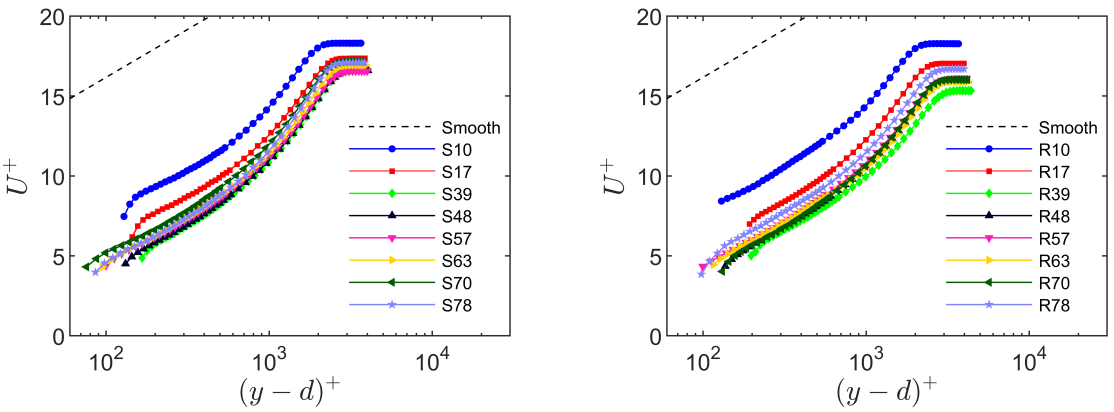

(a) Staggered cases

(b) Random cases

Figure 1: Spatially-averaged mean velocity profiles in inner scaling

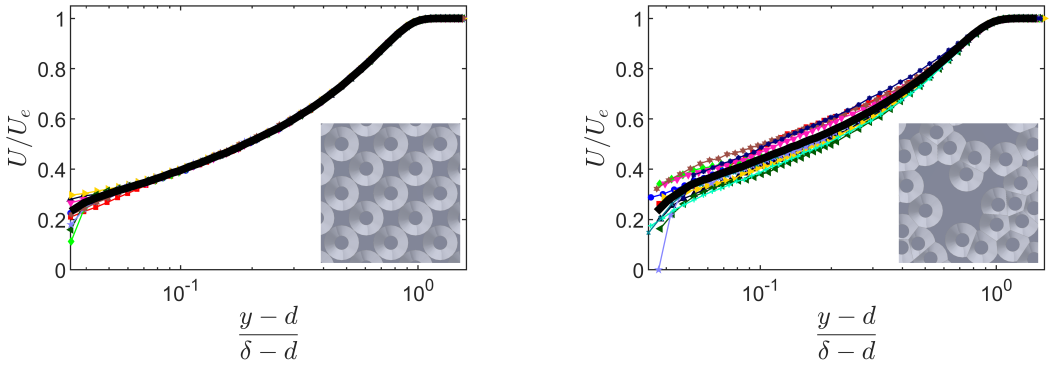

(a) S78 case (b) R78 case

Figure 2: Mean velocity profiles in outer scaling for select cases, with all individual profiles in color. The thick black line is the area-weighted average profile for the case. All similar staggered case plots are consistent with (a), and all similar random case plots are consistent with (b).

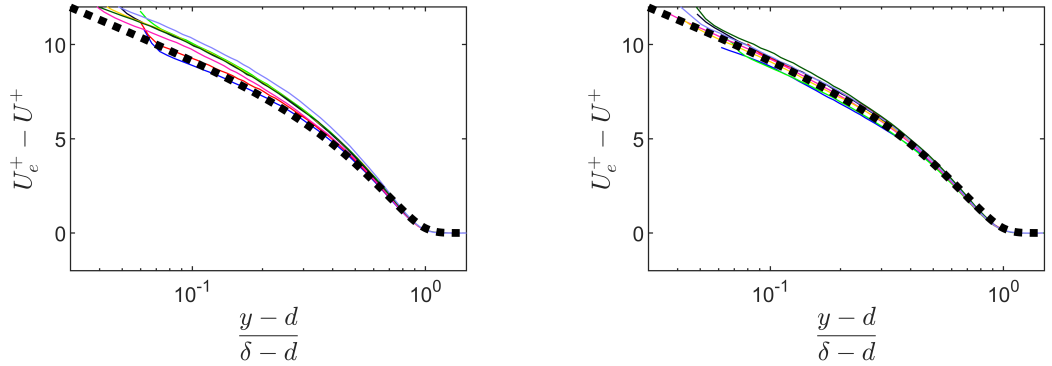

(a) Staggered cases (b) Random cases

Figure 3: Staggered and random cases shown in mean velocity defect form. The thick dotted black line is the smooth-wall DNS result at $\mathrm{Re}_\tau \approx 2000$ from Sillero *et al.* (2013).

defect plot near the wall is in contrast to the random cases' results where more traditional values of wake strength and a tighter spread in the defect plot near the wall was observed. Previous studies, such as Flack *et al.* (2005) among others, point to collapse in the velocity defect plot as a primary indicator of outer-layer similarity. An analysis of only the spatially-averaged profiles here would seem to indicate a breakdown in outer-layer similarity.

Spanwise heterogeneity in random cases

Figure 4 shows all 12 profiles from the R78 case normalized individually with inner scaling determined from the comprehensive shear stress method. d was determined from the spanwise-averaged profile and held constant when analyzing all individual profiles for u_τ and y_0. The lack of collapse of the profiles is striking given that all of these profiles were recorded over a similar surface at the same Reynolds number, $\mathrm{Re}_x = U_e x/\nu$. From other literature like Flack *et al.* (2005) and Placidi & Ganapathisubramani (2015) differences would only be expected in the near-wall region below $5k$. Furthermore, if each of these profiles were examined individually, there would be little evidence that the boundary layer was not consistent across the tunnel's span.

Figure 5 shows the spanwise wall-normal plane of mean streamwise velocity at $x = 1.50\,\mathrm{m}$ surveyed with the LDV on selected cases. These plots show different tests

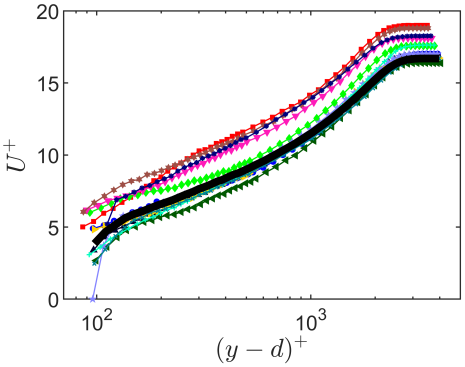

Figure 4: All R78 surface profiles mean streamwise velocity in inner scaling

than were described before and survey the entire tunnel span with linear grid spacings in the y- and z-directions. The smooth wall survey (Fig. 5a) shows very little spanwise heterogeneity as expected. In contrast, both random cases shown in Figs. 5b and 5c and all six other random surfaces not shown display mean streamwise velocity heterogeneity across the span consistent with LMP and HMP observations from other studies such as Barros & Christensen (2014) and

Anderson *et al.* (2015).

Given that the random surfaces show spanwise heterogeneity consistent with LMPs and HMPs, it would perhaps be expected that the regular surfaces would also show spanwise heterogeneity. However, there appears to be no evidence of boundary layer scale spanwise heterogeneity given the collapse of the data in Fig. 2a and other staggered cases not shown. Maybe this should not be surprising, though, since Vanderwel & Ganapathisubramani (2015) show that spanwise heterogeneity was confined to the roughness sublayer when spanwise spacing is less than $\delta/2$ which is larger than adjacent rows in this study.

Figures 5b and 5c show the full range of average element distance tested on the random surfaces with LMPs and HMPs present in all cases. This is especially important to highlight since Vanderwel & Ganapathisubramani (2015) and Anderson *et al.* (2015) have shown evidence of LMPs and HMPs over roughnesses with spanwise heterogeneities spaced at approximately 1δ and greater. The average element spacings here are all below this and considerably so in the R78 case. Additionally, taken together Figs. 5a, 5b, and 5c show that the occurrence of the LMPs and HMPs are likely not due to the tunnel because the smooth-wall case shows little evidence of such flows and because the LMPs and HMPs are present in different locations on the R10 and R78 cases. The difference in LMP and HMP locations are even more evident when looking at tests from the other six random surfaces not shown.

In Fig. 6a, the R78 case full-span linearly-spaced mean streamwise data are shown again in 2D in the upper plot. Overlaid in black is the R78 test which had the 12 profiles described earlier and recorded for all eight random surfaces. Overlaid in red on this figure is an additional test with data at this location which is described in more detail later (see description for Fig. 7). This plot highlights the repeatablity of the LMPs and HMPs by showing that the LMPs and HMPs appear in the same locations on independent test runs.

In Fig. 6b, mean elevation of roughness 1δ immediately upstream of the measurement location, $\langle h \rangle_x$, is plotted in black, and standard deviation of roughness 1δ immediately upstream of the measurement location, $\langle \sigma_h \rangle_x$, is plotted in red. The $\langle h \rangle_x$ and $\langle \sigma_h \rangle_x$ data were low pass filtered with a Fourier cut-off at 0.125δ as in Barros & Christensen (2014). Barros & Christensen (2014) correlated LMPs with relatively low upstream surface elevation and HMPs with relatively higher upstream surface elevation. This does not appear to correlate with LMPs and HMPs in this case. Additionally, Anderson *et al.* (2015) correlated LMPs with relatively lower k spanwise regions and HMPs with relatively higher k spanwise regions. If there was a difference in average peak-to-through distance correlated with LMPs and HMPs here, it would likely be evident in the red plot of standard deviation. However, standard deviation appears relatively consistent across the span.

Figure 6c shows the R78 case full-span Reynolds shear stress data. This plot gives further evidence of LMPs and HMPs since it demonstrates elevated and depressed levels of Reynolds shear stress coincident with LMPs and HMPs respectively as was shown in both Barros & Christensen (2014) and Anderson *et al.* (2015).

Finally, Fig. 7 shows three planes of mean streamwise velocity data for the R78 case. Each of these planes contains six profiles spaced $1.5D$ centered in the span. The middle plane is located at $x = 1.50\,\mathrm{m}$ and is the one shown in red contours in Fig. 6a. The upstream and downstream planes are located $\pm 8\,\mathrm{cm}$, approximately 2δ, from the center plane. The three planes show similar contours which indicates that these repeatable LMPs and HMPs exist longer than 4δ. This indicates that the secondary flow structures creating the LMPs and HMPs are longer-standing than the 1δ noted by Barros & Christensen (2014). Additionally, it would reasonably suggest that the structures in this study should not be correlated with surface statistics calculated from only 1δ upstream. Lastly, Anderson *et al.* (2015) describes TKE production over relatively higher peak-to-trough areas as the driving force creating and sustaining LMPs and HMPs. The statistical homogeneity of this surface and the longevity of the structures suggest that additional mechanisms may be needed to explain the sustainment of the LMPs and HMPs documented here.

CONCLUSION

Differences in mean streamwise velocity profiles recorded over regular arrangements of truncated cone roughness elements were confined below one roughness height above the roughness crests. In contrast to this, mean streamwise velocity profiles recorded over random cases showed marked differences across the span even though they were measured over a similar surface at the same fetch. However, each of these profiles if recorded individually would have little evidence of the differences present across the span.

The differences were found to be indicative of Low Momentum Pathways and High Momentum Pathways and marked by elevated and depressed Reynolds shear stress as seen previously by Barros & Christensen (2014), Vanderwel & Ganapathisubramani (2015), and Anderson *et al.* (2015). However, each of those studies had systematic or regular topography which they show contributed to secondary flows. The analysis highlighted that the surfaces studied here do not appear to have the surface characteristics which may have caused the secondary flows in those previous studies. In fact, to the authors' knowledge this is the first study to observe LMPs and HMPs over a completely random and largely statistically-consistent fetch. Also, the LMPs and HMPs were shown to be repeatable, appearing in the same location for a surface in different test runs. Finally, the LMPs and HMPs were shown to be long-standing, extending downstream to distances greater than 4δ.

This study highlights that the underlying mechanisms which cause secondary flows over rough surfaces are not yet well understood. LMPs and HMPs may be present on random surfaces and current prediction criteria remain insufficient.

REFERENCES

Anderson, W., Barros, J. M., Christensen, K. T. & Awasthi, A. 2015 Numerical and experimental study of mechanisms responsible for turbulent secondary flows in boundary layer flows over spanwise heterogeneous roughness. *Journal of Fluid Mechanics* **768**, 316–347.

Barros, J. M. & Christensen, K. T. 2014 Observations of turbulent secondary flows in a rough-wall boundary layer. *Journal of Fluid Mechanics* **748**, R1.

Flack, K. A., Schultz, M. P. & Shapiro, T. A. 2005 Experimental support for townsends Reynolds number similar-

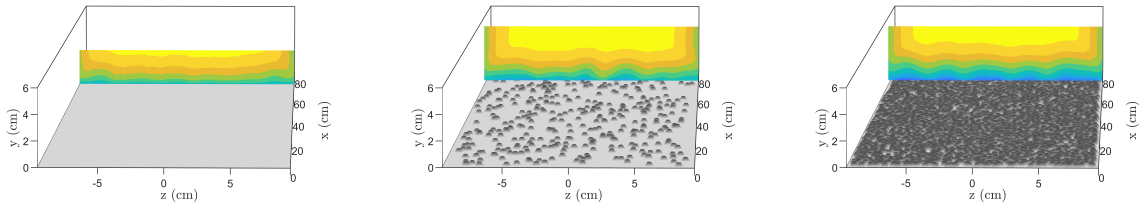

(a) Smooth wall (b) R10 (c) R78

Figure 5: Select surfaces shown in 3D with contour plot of mean streamwise velocity. See Fig. 6a for color scale.

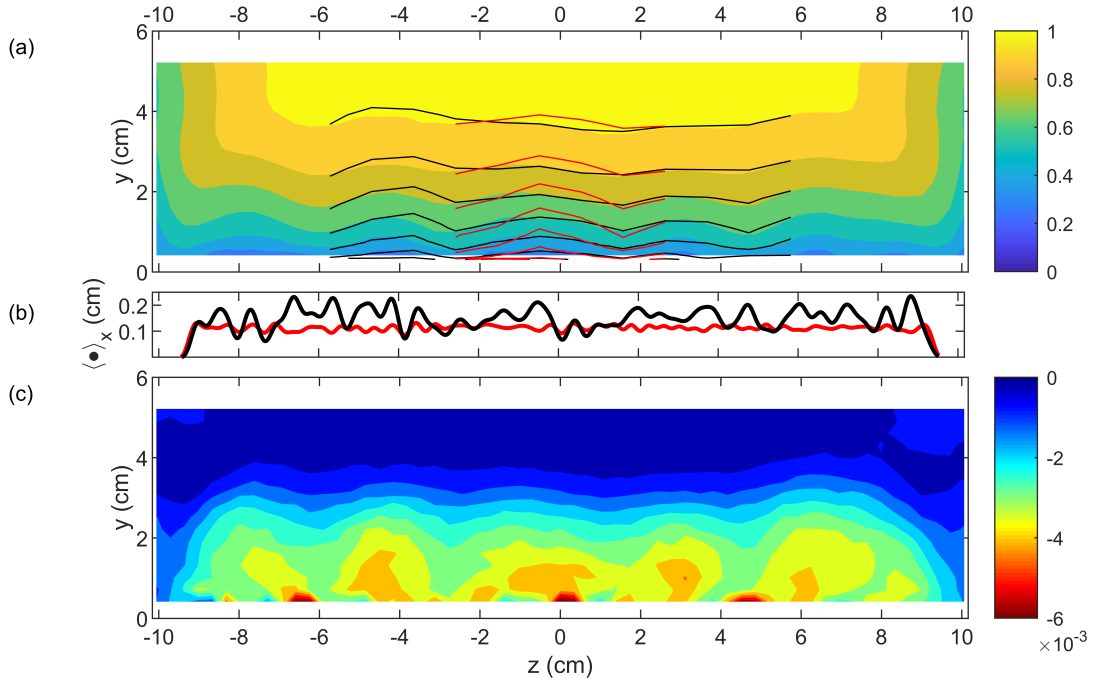

Figure 6: (a) R78 surface mean streamwise velocity, U/U_e, contour plot from three different experiments at $x = 1.50\,\mathrm{m}$. (b) Mean elevation of roughness 1δ immediately upstream of the measurement location, $\langle h \rangle_x$, in black, and standard deviation of roughness 1δ immediately upstream of the measurement location, $\langle \sigma_h \rangle_x$, in red. (c) R78 surface Reynolds shear stress, $\overline{u'v'}/U_e^2$, contour plot from the full span survey.

ity hypothesis on rough walls. *Physics of Fluids* **17** (3), 035102.

Placidi, M. & Ganapathisubramani, B. 2015 Effects of frontal and plan solidities on aerodynamic parameters and the roughness sublayer in turbulent boundary layers. *Journal of Fluid Mechanics* **782**, 541–566.

Sillero, J. A., Jiménez, J. & Moser, R. D. 2013 One-point statistics for turbulent wall-bounded flows at Reynolds numbers up to $\delta^+ \approx 2000$. *Physics of Fluids* **25**, 105102.

Vanderwel, C. & Ganapathisubramani, B. 2015 Effects of spanwise spacing on large-scale secondary flows in rough-wall turbulent boundary layers. *Journal of Fluid Mechanics* **774**, R2.

Volino, R. J. & Schultz, M. P. 2018 Determination of wall shear stress from mean velocity and Reynolds shear stress profiles. *Phys. Rev. Fluids* **3**, 034606.

Womack, K. M., Meneveau, C. & Schultz, M. P. 2019 Comprehensive shear stress analysis of turbulent boundary layer profiles. Submitted to *Journal of Fluid Mechanics*.

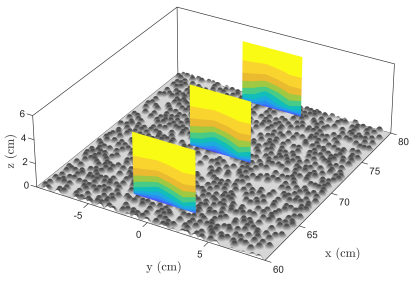

Figure 7: R78 mean streamwise velocity isometric contour plot of three spanwise-wall-normal planes. The center plane is at $x = 1.50\,\mathrm{m}$. The upstream and downstream planes are at $x = 1.50 \pm 0.08\,\mathrm{m}$.